Infrared Vibrational Autodetachment Spectroscopy of Microsolvated Benzonitrile Radical Anions

Toshihiko Maeyama,* Izumi Yagi, Yasuhiro Murota, Asuka Fujii, and Naohiko Mikami*

Department of Chemistry, Graduate School of Science, Tohoku University, Aoba-ku, Sendai 980-8578, Japan

Received: July 12, 2006; In Final Form: November 1, 2006

Vibrational spectra of microsolvated benzonitrile radical anions ($C_6H_5CN^-$−S; S = H_2O and CH_3OH) were measured by probing the electron detachment efficiency in the 3 μm region, representing resonance bands of autodetachment via OH stretching vibrations of the solvent molecules. The hydrogen-bonded OH band for both the cluster anions exhibited a large shift to the lower energy side with approximately 300 cm^{-1} compared to those for the corresponding neutral clusters. The solvent molecules are bound collinearly to the edge of the CN group of the benzonitrile anion in the cluster structures optimized with the density functional theory, in which the simulated vibrational energies are in good agreement with the observed band positions. Natural population analyses were performed for a qualitative implication in changes of solvent orientation upon electron attachment. Asymmetric band shapes depending on the vibrational modes are discussed with respect to dynamics of the autodetachment process from a theoretical aspect incorporated with density functional calculations.

1. Introduction

Solvent reorganization is one of the significant factors predominating electron-transfer reaction rates in the condensed phase.[1] From a viewpoint of the molecular scale, it is still ambiguous how solvent molecules are directed in the course of electron-transfer reactions, because it is quite a task to extract the reorganization of the solvation shell among an infinite number of solvent molecules in a bulk system. However, structural changes of ionized molecular clusters will provide microscopic insights into the solvent reorientation. Although photoelectron spectroscopy inherently informs us of geometrical deviations between the neutral and the ionized clusters, it is always difficult to resolve congested spectra involving intermolecular vibrational bands. Recently, infrared vibrational spectroscopy has revealed ionic cluster structures for both positively and negatively charged species. Nevertheless, structural comparison with the corresponding neutral clusters has been studied intensively for cations[2−4] but scarcely for anions, because most of small molecules with a closed shell have a negative electron affinity under an isolated condition in the gas phase, whereas cations are easily produced by electron impact or photoionization.

Aromatic nitrile compounds are known to play an important role as an electron acceptor in numerous photoinduced electron-transfer reactions.[5] Benzonitrile (BN) is their prototype, whose *valence* electron affinity was reported to be slightly positive.[6−8] The radical anion BN^- in the condensed phase has been investigated by optical absorption,[9] vibrational spectroscopy,[10] and ESR[11] measurements coupled with electrochemistry or pulse radiolysis. Chutny and Swallow[9] reported that the radical anion formed a proton-bound adduct in an acidic aqueous solution. In contrast to lack of studies on gas-phase microsolvation in the anionic state, neutral clusters involving BN have been studied intensively by several groups using LIF,[12] double resonance,[13] and microwave absorption[14] spectroscopic techniques. All the experimental results for BN−H_2O and BN−CH_3OH clusters are consistent with a motif that the solvent molecule attaches to the side of the CN group carrying a large dipole moment.

In the present work, we report photodetachment efficiency spectra of BN^- solvated by a single solvent molecule (H_2O and CH_3OH) in the 3 μm region. Vibrational structures in the OH stretching region were analyzed through resonance bands due to autodetachment in combination with theoretical calculations based on the density functional theory. Structural change upon electron attachment is discussed from an aspect of the electrostatic interaction on the basis of natural population analyses. In addition, the band shapes are analyzed for examining dynamics of the autodetachment process.

2. Experiment

Details of the time-of-flight mass spectrometer and the laser system used in the present work have been described elsewhere.[15,16] Briefly, cluster anions were generated by attachment of photoinduced electrons in a supersonic expansion of sample vapor seeded in neon gas. The generated anion cloud was repelled into a drift tube by a high-voltage pulse and the desired species was separated by a mass gate. The target anions were irradiated by a pulsed infrared light when they reached the photointeraction region in the middle of the drift tube. Photodetached electrons were collected into a closely placed micro-channel plate by a 1 μs square pulse of −15 V. The electron detection is more sensitive for probing the electron detachment process induced by the incident photons than the fast neutral detection[15] contaminated by metastable decay products of hot clusters in the drift tube. The infrared light pulse was obtained by difference frequency generation in a $LiNbO_3$ crystal between the fundamental output of a Nd:YAG laser (Spectra Physics GCR-230) and a dye laser (Lambda Physik Scanmate, LDS759+Styryl9M dyes) pumped by the second harmonic of the same laser. Signal intensities of the target anions and the electrons were simultaneously monitored by a digital oscilloscope (Lecroy Waverunner 6050) operating area integrations of wave forms. These were

* To whom correspondence should be addressed. E-mail: tmaeyama@mail.tains.tohoku.ac.jp (T.M.); nmikami@mail.tains.tohoku.ac.jp (N.M.).

10.1021/jp064389+ CCC: $33.50
Published on Web 12/21/2006

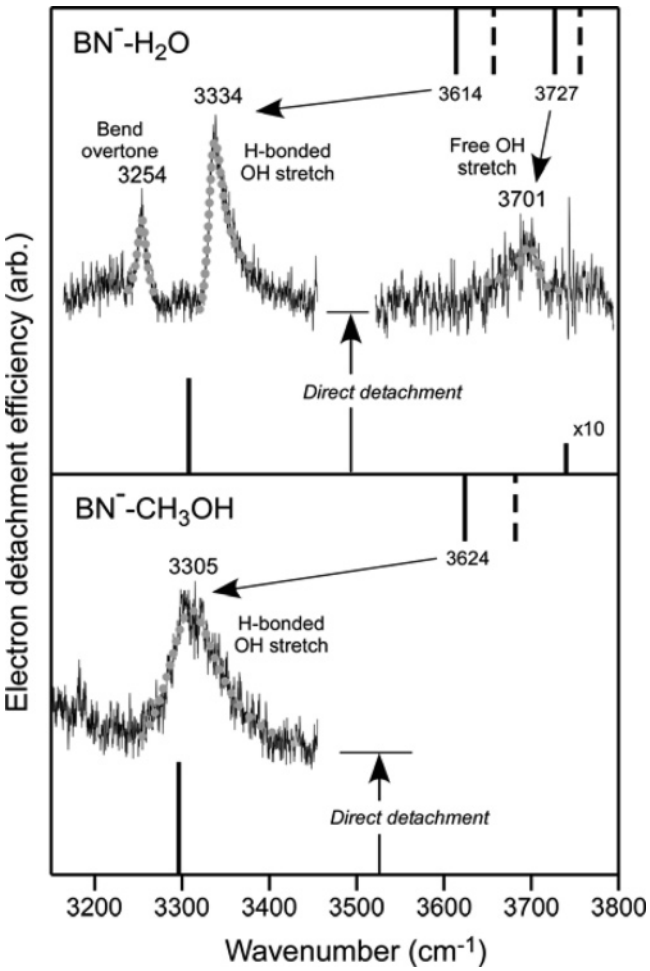

Figure 1. Photodetachment efficiency spectra for BN^--H_2O (upper panel) and $BN^-{-}CH_3OH$ (lower panel). Band positions for the corresponding neutral cluster (solid line) and the bare solvent molecule (broken line) are appended to the top of each panel. Fitted curves to the Fano profiles are represented by gray dotted lines. Simulated spectrum for the anionic state (scaling factor = 0.9632) at the B3LYP/6-31+G(d,p) level is presented on each bottom.

sent to a personal computer accumulating data, which were normalized against synchronously probed infrared light fluence. Because the depletion of the target anion signal did not exceed 5% under present conditions of the light fluence (typically, 1−2 mJ/(pulse·cm^2)), electron detachment efficiencies were normalized also against the anion intensity to cancel the ion source fluctuation.

3. Results and Discussion

Infrared Electron Detachment Spectra as Vibrational Spectra. The upper panel of Figure 1 shows the photodetachment efficiency spectrum of $BN^-{-}H_2O$ in the 3200−3800 cm^{-1} range. In addition to a continuous background due to direct detachment, three resonance bands having asymmetric profiles appear. These band contours are reproduced by least-square fittings to the Fano line shape function,[17] which suggests the interference between the wave functions of the discrete anionic level and the electronic continuum. Similar asymmetric profiles were reported for vibrational autodetachment of water cluster anions.[18] Although details of the band shapes will be mentioned later, here the fitting parameters for resonance energy of these three bands are given as 3254, 3334, and 3701 cm^{-1}, respectively. Because the spectral feature resembles those for the monohydrated halide anions measured by Johnson and co-workers,[19] the bands are readily assigned to the second overtone of the OH bending, the hydrogen (H)-bonded OH stretching, and the free OH stretching, respectively in the same order. The H-bonded OH band shifts 280 cm^{-1} to the lower energy side, compared with that of the neutral correspondent ($BN-H_2O$) measured by Ishikawa et al.[13] Such a large shift implies a considerable enhancement of H-bonding energy upon the electron attachment to BN. Although it is not easy to obtain experimentally the precise bonding energy, energy shifts of the H-bonded OH band of monohydrated anions were reported to show a good empirical correlation with the gas-phase proton affinities (PAs) of the bare anions,[20,21] irrespective of atomic/molecular size or spin multiplicity of the anions. Because the band position for $BN^-{-}H_2O$ lies in between those for $I^-{-}H_2O$ (3385 cm^{-1}) and $Br^-{-}H_2O$ (3270 cm^{-1}),[19] PA of BN^- is estimated to be $PA(I^-) = 1315$ kJ/mol $< PA(BN^-) <$ 1353 kJ/mol $= PA(Br^-)$.[22]

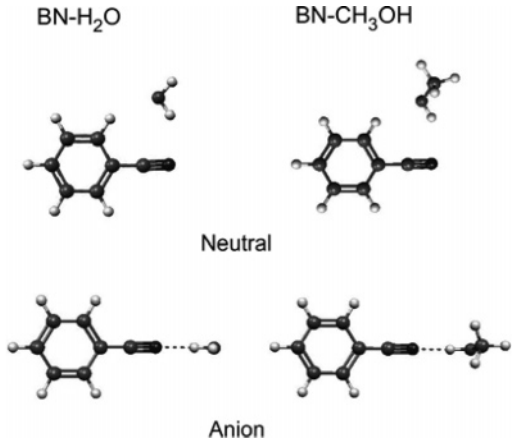

Figure 2. Optimized structures at the B3LYP/6-31+G(d,p) level for $BN-H_2O$ (left) and $BN-CH_3OH$ (right) clusters in the neutral (top) and the anionic (bottom) states.

On the other hand, PA of the neutral BN was reported to be 811.5 kJ/mol.[23] The increase of PA in the anionic state suggests that electron transfer to aromatic nitriles promotes the following proton-transfer reaction in the condensed phase, as was reported by Chutny and Swallow.[9]

The lower panel of Figure 1 shows the photodetachment efficiency spectrum of $BN^-{-}CH_3OH$, which also exhibits a resonance band due to the H-bonded OH stretching accompanied by a continuous background. It is similar to the $BN^-{-}H_2O$ case that a large energy shift representing the enhancement of H-bonding is observed. The resonance energy given by a fit to the Fano profile is 3305 cm^{-1}, which shifts 319 cm^{-1} to the lower energy side from the corresponding band energy in the neutral state. A notable characteristic of $BN^-{-}CH_3OH$ is the extraordinarily broad bandwidth, which is approximately 4 times larger than that of $BN^-{-}H_2O$.

Density Functional Calculations for Determination of the Cluster Structures. In the present work, all the density functional calculations were performed by using the B3LYP level of theory with the 6-31+G(d,p) basis set through the *Gaussian 03* program suite.[24] It has been reported that calculations at the B3LYP/6-31+G(d) level for adiabatic electron detachment energies (ADEs) and vertical detachment energies (VDEs) of aromatic radical anions give an error in the 0.1−0.2 eV range,[25] and that satisfactory optimized geometries for anion−methanol complexes are obtained with the 6-31+G(d,p) basis set.[26] Figure 2 illustrates the optimized structures of the singly solvated benzonitriles in the neutral and the anionic states. The structures in the neutral state, where the solvent molecule

TABLE 1: Adiabatic Electron Detachment Energies (ADE) and Vertical Electron Detachment Energies (VDE) of the Monomer and the H-Bonded Clusters of BN^-

	ADE (eV)		VDE (eV)	
	calc[a]	expt	calc[a]	expt
BN^-	0.235	0.24[b]	0.286	
$BN^-{-}H_2O$	0.553	0.31[c]	0.678	0.50[c]
$BN^-{-}CH_3OH$	0.589		0.680	

[a] Values calculated at the B3LYP/6-31+G(d,p) level. The ADE values are obtained through the zero-point energy correction, whereas the VDE values are calculated as the single-point potential energy differences at the optimized geometries in the anionic state. [b] Temperature dependence of electron attachment equilibrium.[7] [c] Unpublished results of the photoelectron spectrum measured by Mitsui and Nakajima.[27] The experimental ADE value represents the upper limit, which was determined with threshold detachment energy.

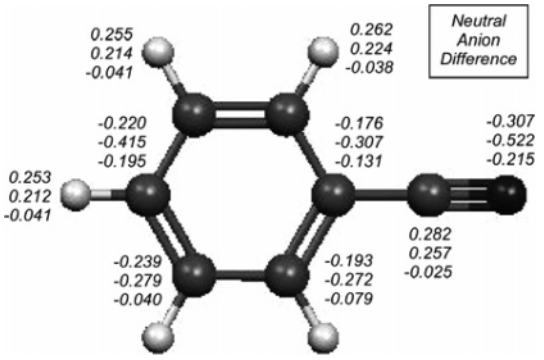

Figure 3. Natural charges on each atom of the benzonitrile molecule at the B3LYP/6-31+G(d,p) level for the neutral (top) and the anionic (middle) states, as well as their difference (bottom).

attaches to the side of the CN group, are similar to those calculated at the Hartree−Fock level.[13] In the anionic state, however, the solvents attach collinearly to the edge of the CN group. The calculational results of ADEs and VDEs for the BN^- monomer and the solvated anions are listed in Table 1. The calculated ADE values for the solvated anions are too high to allow the electron detachment process due to one-photon absorption of the mid-infrared light (0.40−0.46 eV) without internal excitation in the initial state. However, the experimental value for $BN^-{-}H_2O$ measured by Mitsui and Nakajima[27] represents a consistent magnitude with the present observation even if the internal excitation is neglected. The B3LYP level of calculations with a basis set larger than 6-31+G(d) probably tend to overestimate ADEs for H-bonded anions having a small electron binding energy, because a similar upward deviation from the experimental value was reported for the hydrated naphthalene anion system.[28] Simulated vibrational spectra scaled with a factor of 0.9632 are appended to the bottom of each panel in Figure 1, where the band positions fairly reproduce those in experiments except for the bending overtone band originating from intensity borrowing due to Fermi resonance with the stretching mode. The present scaling factor is identical with that proposed for the B3LYP/6-31+G(d,p) level of calculations, taking into account anharmonicity and electron correlation.[29]

Natural populations and electrostatic potentials for the neutral and the anionic BN monomers were analyzed to find a qualitative implication for the solvent orientation. Natural charges and their differences between the neutral and the anionic states are listed in Figure 3. Taking a glance at the differences, one sees that the excess charge is deposited mainly on the nitrogen (N) atom as well as on the carbon atom at the para-position in the benzene ring with respect to the CN group. This

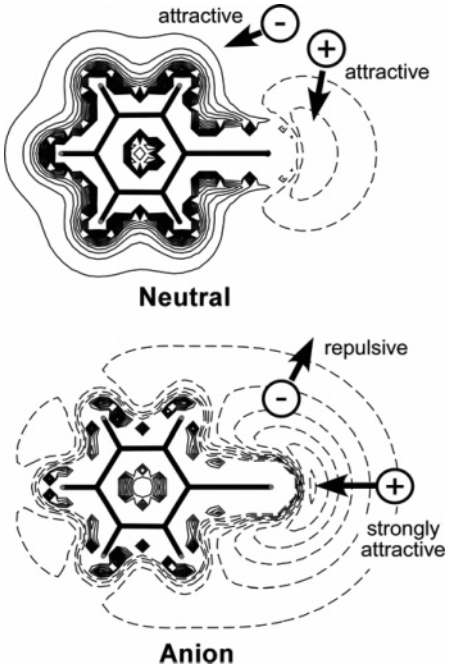

Figure 4. Contour plots for electrostatic potential around the benzonitrile molecule in the neutral (top) and the anionic (bottom) states. Positive and negative contours are represented by solid and broken lines, respectively.

is coincident with a contribution from the quinoid structure proposed by the previous molecular orbital calculation[30] for the result of the ESR study.[11] In the idealized quinoid structure of BN^- with the classical valence treatment, the negative charge localizes on the nitrogen atom as one of paired electrons, and the unpaired electron is located on the para-carbon atom. In fact, a realistic and modern approach via the density functional theory shows the delocalization of the excess charge among the molecule.

Figure 4 shows contour plots of the electrostatic potential around the neutral and the anionic benzonitriles. Although intermolecular forces involving H-bonding should include higher order perturbation terms such as dispersion and charge-transfer contributions, electrostatic interaction is the most effective part to determine the stable cluster geometry. First, considering the situation that a solvent molecule ROH (R = H or CH_3) is placed on the side of the CN group in the neutral state, the negatively charged oxygen atom is attracted to the benzene ring, and a protic H atom of the solvent is attracted to the CN group. Then, it makes the side-attaching form stable. In the anionic state, the oxygen atom undergoes a repulsive force entirely around the BN molecule because of the excess charge delocalization. However, the protic H atom can be trapped in the strongly attractive well on the edge of the nitrogen atom, and hence the collinear form should be the most stable for the anionic clusters.

Dynamical Processes Relevant to the Vibrational Band Shapes. In the present experiment, we only detected the photodetached electron signals, so that we could not discriminate the processes with/without intermolecular bond dissociation. The dissociation energies for the anionic and the neutral $BN{-}H_2O$ cluster are calculated to be 0.447 and 0.130 eV, respectively, at the B3LYP/6-31+G(d,p) level with the BSSE and zero-point energy corrections. Taking into account the experimental ADE values shown in Table 1, the excitation with an infrared photon of 0.40−0.46 eV does not seem to create a sufficiently large excess energy for dissociation before and after electron detachment. Because the photon energy can induce electron detach-

ment without internal excitation in the initial state, we suppose that there is no significant contribution from inhomogeneous spectral broadening, which is frequently exaggerated in infrared dissociation spectroscopy of strongly H-bonded cluster ions.[20] Thus, we analyzed the observed asymmetric band profiles with Fano theory,[17] in which the discrete vibrational states are coupled directly with an electronic continuum. In this framework, the autodetachment lifetime can be determined by fitting parameters of the bandwidth for each vibrational level. These are found to be 390, 270, and 230 fs for the overtone of OH bending, the H-bonded OH stretching, and the free OH stretching of BN^--H_2O, and 70 fs for the H-bonded OH stretching of BN^--CH_3OH, respectively. The lifetime for the free OH level of BN^--H_2O might be underestimated (i.e., the bandwidth would be overestimated) because of an insufficient signal-to-noise ratio in the infrared frequency range covering absorption lines of water vapor, which could not be thoroughly eliminated by a dry nitrogen purge to the optical path. Comparing the two bands of the rest for BN^--H_2O, however, shows that the bandwidth depends upon the vibrational modes.

Another factor to affect the vibrational band shapes is supposed to be *intracluster* vibrational redistribution (IVR). The IVR rates for neutral H-bonded clusters of aromatic molecules have been measured in real time by using picosecond infrared−ultraviolet double resonance spectroscopy.[31,32] It has been reported that the lifetime of a coherently excited vibrational level can be as short as 1 ps for a moderately H-bonded system such as the neutral phenol dimer.[32] For the present system with a strong ionic H-bond, therefore, the IVR rate might compete with the autodetachment rate in the same subpicosecond time domain. An asymmetric band shape due to autodetachment originates from phase shifts of the wave functions of the detached electron, whereas the IVR process does not give such phase shifts because it occurs in the same electronic bound state. Actually, the OH bending overtone band of BN^--H_2O exhibits a near-symmetric profile. In this case, it is possible that the band shape is determined by the IVR rate when the IVR is followed by slow autodetachment. It should be noted for the case of BN^--CH_3OH that the IVR process would be accelerated by a bunch of low-frequency vibrations involving the intermolecular modes with a larger reduced mass as well as the internal rotation of the methyl group. The band profile probably has to be evaluated as a consequence of the convolution of the nonadiabatic and the anharmonic couplings, so that the experimentally determined lifetime should be regarded as the *lower limit* for the real autodetachment process.

Theoretical Aspect of the Mode-Dependent Autodetachment Dynamics. Finally, we suggest a possibility of vibrational mode dependence in the autodetchment process from a theoretical aspect incorporated with density functional calculations. Formalizations of the nonadiabatic coupling[33−35] have been proposed for internal conversion of neutral excited molecules. The internal conversion matrix element is factored into the product of two parts, one is the reciprocal of the difference between the potential energies of the two electronic states, and the other is concerned with the first derivative of potential energies with respect to a normal vibrational coordinate. Hence, a vibrational coordinate affecting the difference potential energy between the two electronic states should cause a large coupling matrix element. The matrix element for vibrational autodetachment is expressed in a similar manner, even if the final state is a continuum in this case. Simons proposed propensity rules[36] for autodetachment rates of vibrationally excited anions. For the case of electron detachment, the difference potential energy

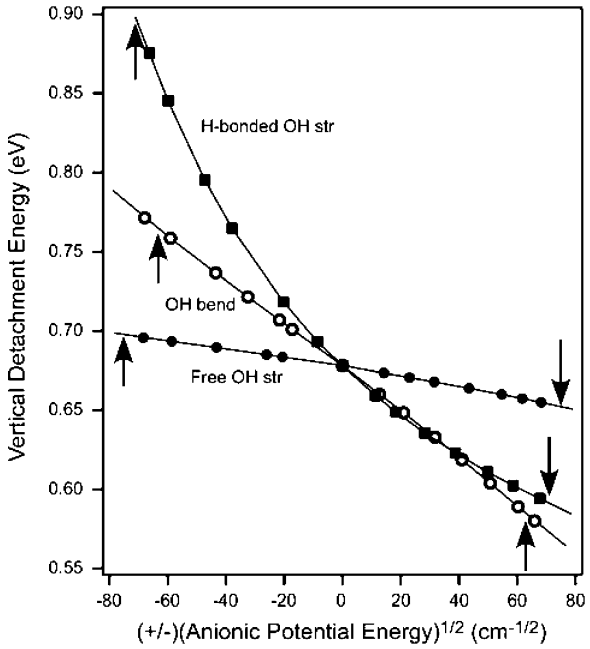

Figure 5. Vertical electron detachment energy of BN^--H_2O calculated at the B3LYP/6-31+G(d,p) level as a function of signed square roots of the anionic potential energy deviations due to nuclear displacements along the solvent vibrational coordinates (closed square: H-bonded OH stretch, open circle: OH bend, closed circle: free OH stretch). Arrows indicate the classical turning points of $v = 1$ for the OH stretching modes and $v = 2$ for the bending mode, respectively.

is given by the vertical detachment energy as a function of nuclear displacement along vibrational coordinates. Figure 5 shows plots of the calculated VDE values for BN^--H_2O with respect to the solvent vibrational coordinates. The horizontal axis of the plots represents the signed square root values of deviations of the anionic potential energy, which is proportional to the nuclear displacements under the harmonic approximation. The negative and positive signs exhibit displacements to the opposite directions, corresponding to the inner and the outer motions with respect to the distance between the N atom and the H-bonded H atom. The VDE function along the H-bonded OH stretching coordinates shows a curved dependence with the steepest slope at the stationary point, and the other coordinates exhibit linear dependences representing small changes of force constants between the anionic and the neutral state. It should be noted that the slope for the bending coordinate is reduced to be almost half relatively if nondimensional normal coordinates are adopted as the horizontal axis, because the bending mode frequency is nearly a half of the stretching modes.

Because the nonadiabatic coupling matrix element is essentially the first derivative product of the initial and final wavefunctions with respect to the normal coordinates, the VDE functions above should originate from deformation of the wave function of the excess electron, reflecting natural charge distributions among the atoms involved in the vibration. According to natural population analyses on the BN^- clusters in the optimized structures (see Supporting Information in comparison with the values given in Figure 3), approximately 30% of the excess charge is accommodated to the ROH−N atomic group, where 25% and 4−5% of the charge are distributed for the nitrogen atom and the ROH, respectively. Table 2 shows deviations of natural charges for the ROH−N group at the classical turning points of zero-point vibrations, where the amplitudes of vibrational wave functions for a few quanta are large enough. For BN^--H_2O, the largest change is found for charge transfer (CT) character of the H_2O moiety

TABLE 2: Deviations of Natural Charges for the ROH−N Group at the Classical Turning Points for Zero-Point Vibrations Relative to the Stationary Point Values

	nitrogen atom		ROH (total)	
	inner turning point	outer turning point	inner turning point	outer turning point
BN^--H_2O	(−0.57964)[a]		(−0.04379)[a]	
free OH str	+0.00022	−0.00007	+0.00279	−0.00225
H-bonded OH str	+0.00434	−0.00053	−0.03560	+0.01893
OH bend	+0.00107	+0.00124	−0.00630	+0.00417
BN^--CH_3OH	(−0.58176)[a]		(−0.05225)[a]	
H-bonded OH str	+0.00186	−0.00110	−0.03564	+0.02100

[a] Values in parentheses are the natural charges at the stationary points.

affected by the H-bonded OH stretching mode, surprisingly ranging from 2.5 to 7.9% in the zero-point level! Such a large change of the electron distribution should induce a significant enhancement of the nonadiabatic coupling matrix element. The broad band of BN^--CH_3OH could be explained in part by the reason that the CH_3OH moiety has a larger CT character ranging from 3.1 to 8.8%, which is expected to promote the interaction between the electron and vibration of the solvent molecule.

4. Conclusions

Vibrational bands of solvent molecules have been observed in the infrared electron detachment efficiency spectra of the microsolvated benzonitrile anions. The H-bonded OH stretching bands exhibit a large shift to the lower energy side, which implies formation of a strong H-bond formation. The band positions were reproduced with harmonic frequency calculations for the collinear structures optimized at the B3LYP/6-31+G-(d,p) level. The electrostatic potential around the BN monomer anion evidently shows the stability of the collinear attaching of the solvent molecule.

The asymmetric band profiles were analyzed to determine the autodetachment lifetime within a framework of the Fano theory. The mode dependence of the nonadiabatic coupling was examined with calculations of potential energy and natural charges altered along the vibrational coordinates of the solvent, and the H-bonded OH stretching mode was suggested to promote the coupling effect. Nevertheless, we pointed out that the band widths give only the lower limit of the lifetime when the IVR process competes with the detachment in the femtosecond time domain. In fact, such a discussion will be more plausible after a comprehensive determination of the IVR rates for strongly H-bonded anionic systems.

Acknowledgment. We thank Dr. Y. Matsuda and Dr. M. Sugiyama for valuable discussions. Dr. M. Mitsui and Prof. A. Nakajima at Keio University are gratefully acknowledged for providing us with unpublished results of photoelectron spectroscopy of BN^--H_2O. This work is supported by the Grant-in-Aid for Specifically Promoted Research (No. 16002006) from the Ministry of Education, Culture, Sports, Science, and Technology of Japan.

Supporting Information Available: Natural populations for BN^-, $BN^-−H_2O$, and $BN^-−CH_3OH$ anions are calculated at the B3LYP/6-31+G(d,p) level. This material is available free of charge via the Internet at http://pubs.acs.org.

References and Notes

(1) Kosower, E. M.; Huppert, D. *Annu. Rev. Phys. Chem.* **1986**, *37*, 127.
(2) Miyazaki, M.; Fujii, A.; Ebata, T.; Mikami, N. *Chem. Phys. Lett.* **2001**, *349*, 431.
(3) Fujii, A.; Ebata, T.; Mikami, N. *J. Phys. Chem. A* **2002**, *106*, 8554.
(4) Enomoto, S.; Miyazaki, M.; Fujii, A.; Mikami, N. *J. Phys. Chem. A* **2005**, *109*, 9471.
(5) Kavarnos, G. J. *Fundamentals of Photoinduced Electron Transfer*; Wiley-VCH: New York, 1993.
(6) Wentworth, W. E.; Kao, L. W.; Becker, R. S. *J. Phys. Chem.* **1975**, *79*, 1161.
(7) Zlatkls, A.; Lee, C. K.; Wentworth, W. E.; Chen, E. C. M. *Anal. Chem.* **1983**, *55*, 1596.
(8) Burrow, P. D.; Howard, A. E.; Johnston, A. R.; Jordan, K. D. *J. Phys. Chem.* **1992**, *96*, 7570.
(9) Chutny, B.; Swallow, A. J. *Trans. Faraday Soc.* **1970**, *66*, 2847.
(10) Dimitrova, Y. *THEOCHEM* **1997**, *391*, 241.
(11) Ludwig, P.; Adams, R. N. *J. Chem. Phys.* **1962**, *37*, 828.
(12) Kobayashi, T.; Honma, K.; Kajimoto, O.; Tsuchiya, S. *J. Chem. Phys.* **1987**, *86*, 1111.
(13) Ishikawa, S.; Ebata, T.; Mikami, N. *J. Chem. Phys.* **1999**, *110*, 9504.
(14) Melandri, S.; Consalvo, D.; Caminati, W.; Favero, P. G. *J. Chem. Phys.* **1999**, *111*, 3874.
(15) Kawamata, H.; Maeyama, T.; Mikami, N. *Chem. Phys. Lett.* **2003**, *370*, 535.
(16) Maeyama, T.; Negishi, Y.; Tsukuda, T.; Yagi, I.; Mikami, N. *Phys. Chem. Chem. Phys.* **2006**, *8*, 827.
(17) Fano, U. *Phys. Rev.* **1961**, *124*, 1866.
(18) Ayotte, P.; Weddle, G. H.; Bailey, C. G.; Johnson, M. A.; Vila, F.; Jordan, K. D. *J. Chem. Phys.* **1999**, *110*, 6268.
(19) Ayotte, P.; Weddle, G. H.; Kim. J.; Johnson, M. A. *J. Am. Chem. Soc.* **1998**, *120*, 12361.
(20) Robertson, W. H.; Johnson, M. A. *Annu. Rev. Phys. Chem.* **2003**, *54*, 173.
(21) Roscioli, J. R.; Diken, E. G.; Johnson, M. A.; Horvath, S.; McCoy, A. B. *J. Phys. Chem. A* **2006**, *15*, 4943.
(22) *NIST Chemistry WebBook* (http://webbook.nist.gov/chemistry/); National Institute of Standards and Technology: Gaithersburg, MD, 2005.
(23) Hunter, E. P.; Lias, S. G. *J. Phys. Chem. Ref. Data* **1998**, *27*, 413.
(24) Frisch, M. J.; Trucks, G. W.; Schlegel, H. B.; Scuseria, G. E.; Robb, M. A.; Cheeseman, J. R.; Montgomery, J. A., Jr.; Vreven, T.; Kudin, K. N.; Burant, J. C.; Millam, J. M.; Iyengar, S. S.; Tomasi, J.; Barone, V.; Mennucci, B.; Cossi, M.; Scalmani, G.; Rega, N.; Petersson, G. A.; Nakatsuji, H.; Hada, M.; Ehara, M.; Toyota, K.; Fukuda, R.; Hasegawa, J.; Ishida, M.; Nakajima, T.; Honda, Y.; Kitao, O.; Nakai, H.; Klene, M.; Li, X.; Knox, J. E.; Hratchian, H. P.; Cross, J. B.; Bakken, V.; Adamo, C.; Jaramillo, J.; Gomperts, R.; Stratmann, R. E.; Yazyev, O.; Austin, A. J.; Cammi, R.; Pomelli, C.; Ochterski, J. W.; Ayala, P. Y.; Morokuma, K.; Voth, G. A.; Salvador, P.; Dannenberg, J. J.; Zakrzewski, V. G.; Dapprich, S.; Daniels, A. D.; Strain, M. C.; Farkas, O.; Malick, D. K.; Rabuck, A. D.; Raghavachari, K.; Foresman, J. B.; Ortiz, J. V.; Cui, Q.; Baboul, A. G.; Clifford, S.; Cioslowski, J.; Stefanov, B. B.; Liu, G.; Liashenko, A.; Piskorz, P.; Komaromi, I.; Martin, R. L.; Fox, D. J.; Keith, T.; Al-Laham, M. A.; Peng, C. Y.; Nanayakkara, A.; Challacombe, M.; Gill, P. M. W.; Johnson, B.; Chen, W.; Wong, M. W.; Gonzalez, C.; Pople, J. A. *Gaussian 03*, Gaussian, Inc.: Wallingford, CT, 2004.
(25) Modelli, A.; Mussoni, L.; Fabbri, D. *J. Phys. Chem. A* **2006**, *110*, 6482.
(26) Koné, M.; Illien, B.; Graton, J.; Laurence, C. *J. Phys. Chem. A* **2005**, *109*, 11907.
(27) Mitsui, M.; Nakajima, A. Private Communication.
(28) Schiedt, J.; Knott, W. J.; Le Barbu, K.; Schlag, E. W.; Weinkauf, R. *J. Chem. Phys.* **2000**, *113*, 9470.
(29) Irikura, K. K.; Johnson, R. D., III; Kacker, R. N. *J. Phys. Chem. A* **2005**, *109*, 8430.
(30) Drago, R. S.; Petersen, H., Jr. *J. Am. Chem. Soc.* **1967**, *89*, 3978.
(31) Ebata, T.; Kayano, M.; Sato, S.; Mikami, N. *J. Phys. Chem. A* **2001**, *105*, 8623.
(32) Kayano, M.; Ebata, T.; Yamada, Y.; Mikami, N. *J. Chem. Phys.* **2004**, *120*, 7410.
(33) Bixon, M.; Jortner, J. *J. Chem. Phys.* **1968**, *48*, 715.
(34) Negri, F.; Orlandi, G.; Zerbetto, F.; Zgierski, M. Z. *J. Chem. Phys.* **1989**, *91*, 6215.
(35) Nagase, H.; Kuki, M.; Zhang, J.-P.; Sashima, T.; Mukai, Y.; Koyama, Y. *J. Phys. Chem. A* **2000**, *104*, 4155.
(36) Simons, J. *J. Am. Chem. Soc.* **1981**, *103*, 3971.